

See discussions, stats, and author profiles for this publication at: <https://www.researchgate.net/publication/221865723>

# Morphology Control of Cadmium Selenide Nanocrystals: Insights into the Roles of Di-n-octylphosphine Oxide (DOPO) and Di-n-octylphosphinic Acid (DOPA)

ARTICLE *in* JOURNAL OF THE AMERICAN CHEMICAL SOCIETY · MARCH 2012

Impact Factor: 12.11 · DOI: 10.1021/ja300135c · Source: PubMed

---

CITATIONS

31

---

READS

73

## 2 AUTHORS, INCLUDING:



Fudong Wang

Washington University in St. Louis

37 PUBLICATIONS 1,189 CITATIONS

SEE PROFILE



# NIH Public Access

## Author Manuscript

*J Am Chem Soc.* Author manuscript.

Published in final edited form as:

*J Am Chem Soc.* 2012 March 21; 134(11): 5369–5380. doi:10.1021/ja300135c.

## Morphology Control of Cadmium Selenide Nanocrystals: Insights into the Roles of Di-*n*-octylphosphine Oxide (DOPO) and Di-*n*-octylphosphinic Acid (DOPA)

Fudong Wang and William E. Buhro

Department of Chemistry and Center for Materials Innovation, Washington University, Saint Louis, Missouri 63130-4899.

### Abstract

Di-*n*-octylphosphine oxide (DOPO) and di-*n*-octylphosphinic acid (DOPA), as two of impurities found in commercial tri-*n*-octylphosphine oxide (TOPO), generate significant differences in the outcomes of CdSe-nanocrystal (NC) syntheses. Using *n*-tetradecylphosphonic acid (TDPA) as the primary acid additive, quantum dots (QDs) are grown with DOPO added, whereas quantum rods (QRs) are grown in the presence of DOPA. While using oleic acid (OA) as the primary acid additive, QDs are generated and the QDs produced with DOPA exhibit larger sizes and size distributions than those produced with DOPO.  $^{31}\text{P}$  NMR analyses of the reaction mixtures reveal that the majority of the DOPO has been converted into DOPA and di-*n*-octylphosphine (DOP) with DOP being removed via evacuation over the course of Cd-precursor preparation. The origin of the puzzling differences in the shape control of CdSe NCs in the presence of DOPO and DOPA is elucidated to be the small quantity of DOPO present, which liberates DOP during NC synthesis. In the presence of DOP, regardless of DOPA, the precursor-conversion kinetics and thus the nucleation kinetics are dramatically accelerated, generating a large number of nuclei by consuming a significant amount of CdSe nutrients, favoring QD growth. Similarly, QD growth is favored by the fast nucleation kinetics in the presence of OA, and the broader size distributions of QDs with DOPA are due to a second nucleation event initiated by the more stable Cd-di-*n*-octylphosphinate component. In contrast, a slow nucleation event results in the growth of QRs in the case of using DOPA and TDPA, where no DOPO or DOP is present. The results thus demonstrate the important role of precursor-conversion kinetics in the control of NC morphologies.

### Introduction

We report the first systematic study of the roles of di-*n*-octylphosphine oxide (*n*-octyl<sub>2</sub>P(O)H, DOPO) and di-*n*-octylphosphinic acid (*n*-octyl<sub>2</sub>P(O)OH, DOPA) in the growth

---

Correspondence to: Fudong Wang; William E. Buhro.

Corresponding Author fwang@wustl.edu, buhro@wustl.edu..

#### ASSOCIATED CONTENT

**Supporting Information.** Methods for TEM, XRD, extinction and PL spectroscopy, mass spectrometry, and CdSe-NC purification and surface-ligand characterization, syntheses and characterizations of DOPA anhydride and *O*-(trimethylsilyl)-di-*n*-octylphosphinic acid (ODOPA), mass spectra of recovered surface ligands of CdSe NCs, calculations of the relative numbers of NCs (grown using the TDPA-and-TOPO protocol with DOPA or DOPO) with respect to control, TEM images of CdSe NCs grown using the TDPA-and-TOPO protocol at early times of reactions and grown using the OA-and-TOPO protocol, XRD patterns of CdSe NCs, extinction and PL spectra of CdSe NCs at various reaction times, additional temporal evolution of PL peak position, PL fwhm, and PL QY of CdSe NCs,  $^{31}\text{P}$  NMR spectra for assignments of Cd-TDPA complex, DOPA, DOPA anhydride, and DOP, additional  $^{31}\text{P}$  NMR spectra of the reaction mixtures of CdSe NCs,  $^{31}\text{P}$  NMR spectra of the surface ligands of CdSe NCs,  $^{31}\text{P}$  NMR spectra of 90% and 97% TOP. This material is available free of charge via the Internet at <http://pubs.acs.org>.

kinetics and morphology control of CdSe nanocrystals (NCs). The striking difference in the shape control of CdSe NCs using DOPA and DOPO rests in the dramatically different nucleation and growth kinetics conferred by DOPA and di-*n*-octylphosphine (*n*-octyl<sub>2</sub>PH, DOP), which is converted from DOPO. The molecular roles of DOPA and DOP in NC nucleation and growth are proposed and the direct correlations between nucleation and growth kinetics and morphology control of NCs are determined. We propose that the control of nucleation and growth kinetics provides a means for the morphology control of colloidal semiconductor NCs having intrinsically anisotropic crystal structures.

Synthesis of colloidal semiconductor NCs has been extensively investigated and significantly advanced,<sup>1-27</sup> since an organometallic synthesis of CdE (E = S, Se, and Te) quantum dots (QDs) using tri-*n*-octylphosphine (*n*-octyl<sub>3</sub>P, TOP) and tri-*n*-octylphosphine oxide (*n*-octyl<sub>3</sub>PO, TOPO) solvent mixtures was introduced.<sup>28</sup> Among the noted advances has been the achievement of morphology control of NCs (quantum rods (QRs) and tetrapods vs. QDs),<sup>1,3</sup> which initiated extensive subsequent research activities and interest in QRs and tetrapods. Growth of QRs and tetrapods has been proposed to be due to preferential binding of ligands (e.g., alkylphosphonic acids, alkylP(O)(OH)<sub>2</sub>) to specific facets of growing NCs, which inhibits growth on those facets and allows growth on other facets (i.e., the (001) facet of wurtzite CdSe).<sup>3,19,29-32</sup> Alternatively, nucleation and growth kinetics determined by the reactivities of the precursors may have a direct link to the morphology control.<sup>1,13,21,33-35</sup> Peng and coworkers proposed that the use of less reactive Cd-alkylphosphonate complexes (as compared to the more reactive Cd-alkylcarboxylate complexes that favor CdSe QD growth) dramatically decreased the numbers of nuclei formed in CdSe QR syntheses, allowing high monomer or nutrient concentrations to be attained, favoring anisotropic growth.<sup>21,34</sup> (We prefer “nutrient” to “monomer” as “nutrient” is a more precise term to describe a solution species (i.e., monomer, dimer, etc.) produced by the precursor reaction that has not undergone nucleation or addition to NCs.<sup>36</sup>)

Another significant advance has been the elucidation of the chemical pathways for the NC formation, in particular the pathways by which the nutrients are generated,<sup>36-40</sup> constituting an important step toward understanding the complex chemistry associated with nucleation and growth. Such mechanisms (Scheme 1) involve a Lewis-acid-activation step, where (taking the synthesis of CdSe NCs as an example) alkylphosphine selenide (R<sub>3</sub>PSe) binds to Cd(OX)<sub>2</sub> (OX<sup>-</sup> = alkylcarboxylate or alkylphosphonate), being thus activated toward nucleophilic attack by OX<sup>-</sup> and P=E bond cleavage, resulting in alkyl-phosphine oxide (R<sub>3</sub>PO) and acid anhydride (XOX).<sup>36,38</sup> (Whether binding or cleavage is the rate-determining step is unclear.) The reaction kinetics depend on the structures of R<sub>3</sub>PSe and Cd(OX)<sub>2</sub>. Sterically hindered triisopropylphosphine selenide<sup>38</sup> and aryl substituted tertiary phosphine selenides<sup>36</sup> exhibit slow kinetics, whereas secondary phosphine selenides (dialkyl- or diphenyl-phosphine selenide) show fast kinetics.<sup>37,39,41</sup> Cd-alkylphosphonate precursors exhibited slower kinetics than Cd-alkylcarboxylate precursors, due to lower Lewis acidities of Cd-alkylphosphonate complexes because of the polydentate coordination and bridging tendencies of alkylphosphonate ligands, which enhance coordinative saturation.<sup>38</sup>

Such significant advances have initiated extensive research activities and interest in the fundamental properties of NCs that have in turn generated many potential technical applications. However, there are still challenges that require significant efforts to meet, one of which is associated with the nucleation and growth of NCs.<sup>43-45</sup> The mechanistic formation of nutrients has been studied as mentioned above and the precursor conversion (to release nutrients) was observed to be equal to the yield of crystalline materials, and the initial rate of the precursor conversion was proportional to the final number of nuclei.<sup>36</sup> However, the intermediates or transition states associated with the nutrient formation and the

mechanistic processes underlying the reactions of nutrients to form nuclei and further to form NCs are still not well understood.

Another big issue is associated with the irreproducibility of the NC syntheses. Colloidal NCs are generally prepared in organic-solvent media containing reagents that are often not highly pure. The variations in the concentrations and identities of the active impurities present often result in different growth kinetics and uncontrolled morphologies. A typical example is TOPO, a popular and important solvent in the NC synthesis, commercially available as 90%- or 99%-purity grade. Its use has resulted in synthetic irreproducibility for CdSe QDs,<sup>7,46-49</sup> CdSe QRs,<sup>1,49-52</sup> CdSe and CdTe hyperbranched NCs,<sup>53</sup> and CdSe quantum wires (QWs).<sup>42</sup>

Although efforts have been made to improve the synthetic reproducibility of NCs by using purified TOPO or other reagents,<sup>6,16,17,20,21,23,36-39,41-44,49,54</sup> a full understanding of the roles of impurities in the syntheses is important to both fundamental mechanistic studies and synthetic-methodology development. For example, alkylphosphonic acids (i.e., *n*-octylphosphonic acid, octylP(O)(OH)<sub>2</sub>, a prominent impurity in TOPO) were responsible for the discovery of QRs, and their roles have been the subject of study for many years.<sup>1-3,18,19,22,29-35,49,51,52,55,56</sup> We previously identified the impurities in commercial TOPO and determined their effects on CdSe QW growth. We showed that DOPA was the important beneficial TOPO impurity for the reproducible growth of high-quality CdSe QWs and the role it played was its ability to beneficially modify precursor reactivity through ligand substitution.<sup>42</sup> In a separate, preliminary communication, we reported that DOPA and mono-*n*-octylphosphinic acid (*n*-octylP(O)(H)OH, MOPA) assisted CdSe QR growth, whereas DOPO enhanced QD growth.<sup>49</sup> However, the spectroscopic data associated with the growth kinetics were not reported and the roles of these TOPO impurities in the morphology control of CdSe NCs were not understood.

The primary goal of this work is to explore the roles and mechanisms of DOPA and DOPO in the growth kinetics and morphology control of CdSe NCs. We adopted established syntheses<sup>11,14,38</sup> and employed *n*-tetradecylphosphonic acid (*n*-tetradecylP(O)(OH)<sub>2</sub>, TDPA) or oleic acid (OA) as the primary acid additive, with smaller amounts of DOPO or DOPA added, to dissolve CdO to form the Cd precursors. In the presence of TDPA, the morphology control is consistent with our previous study:<sup>49</sup> QDs were generated with DOPO added, whereas QRs were produced with DOPA added. When OA was present as the primary acid additive, however, QDs were produced and the QDs made with DOPA exhibited larger sizes and broader size distributions than those made with DOPO. The mechanism for such different synthetic outcomes is elucidated to be due to the dramatic variation of precursor-conversion kinetics caused by the additives. We expect that the knowledge gained through this study will allow more rational syntheses of colloidal semiconductor NCs with desired morphologies and optical properties.

## Experimental Section

### Materials

Tri-*n*-octylphosphine (TOP, 90% and 97%, Aldrich), amorphous selenium shot (Se, 99.999%, Alfa Aesar), cadmium oxide (CdO, 99.99%, Aldrich), *n*-tetradecylphosphonic acid (TDPA, 99%, Polycarbon Industries), 1-octadecene (ODE, 90%, Aldrich), hydrogenated poly(1-decene) (PDE, Aldrich), bis(trimethylsilyl) sulfide ((Me<sub>3</sub>Si)<sub>2</sub>S, synthesis grade, Aldrich), *n*-octylamine (99%, Aldrich), lithium aluminum hydride (LiAlH<sub>4</sub>, 95%, Aldrich), Coumarin 6 (>99%, Aldrich), and Rhodamine 6G (99%, Aldrich) were used as received. Tri-*n*-octylphosphine oxide (TOPO, 99%) was purchased from Aldrich, and purified through recrystallization from acetonitrile as previously described.<sup>42,49</sup> DOPA and

DOPO were synthesized as previously described.<sup>42,49</sup> The TOPSe stock solution (2.0 mmol/g solution) was prepared by dissolving Se (6.0 g, 0.076 mol) into TOP (32.0 g, 0.086 mol) with stirring at room temperature in a glove box. Tetrahydrofuran (THF, ≥ 99.0%, Aldrich) was distilled over Na/benzophenone ketyl. All synthetic procedures for CdSe NCs described below were conducted under dry, O<sub>2</sub>-free N<sub>2</sub> (g).

### Synthesis of CdSe NCs using the TDPA-and-TOPO/ODE/PDE protocol

The procedure was adapted from Peng and Alivisatos and coworkers.<sup>14,38</sup> Briefly, CdO (51 mg, 0.397 mmol), TDPA (223 mg, 0.801 mmol), purified TOPO (3.80 g, 9.83 mmol) or ODE/PDE (3.80 g), and DOPA (0–200 mg, 0–0.689 mmol) or DOPO (0–200 mg, 0–0.729 mmol) were loaded into a 50-mL Schlenk reaction tube. The mixture was degassed under vacuum (0.1–0.2 torr) at 120 °C for 40 min, back-filled with N<sub>2</sub>, and then inserted into a 320 °C salt bath (NaNO<sub>3</sub>/KNO<sub>3</sub>, 46:54 by weight) to achieve a clear and colorless solution (8 min). After further degassing (referred to as the second degassing process) under vacuum (0.1–0.2 torr) at 150 °C (120 °C for ODE) for 1 h, the tube was back-filled with N<sub>2</sub> and switched to a 275 °C salt bath in which the temperature was allowed to equilibrate for 5 min. A TOPSe stock solution (0.30 g, 0.60 mmol) and TOP (0.70 g, 1.89 mmol) (and DOP (25 mg, 0.097 mmol) in two syntheses, see Results) were combined in a separate vial and then loaded into a 3-mL syringe. Once the temperature of the mixture in the tube was stabilized, the mixture of TOPSe and TOP (and DOP) was quickly injected into the tube. Immediately after the injection, the tube was quickly switched to a 250 °C salt bath for subsequent growth. The amount of TOPSe (0.53 ± 0.02 mmol) and TOP (1.75 ± 0.05 mmol) (and DOP (22–23 mg, 0.085 mmol)) injected was measured as the difference between masses of the syringe before and after the injection. Aliquots (~0.1 mL) were taken at various time intervals after the injection of TOPSe and quenched with 1-mL toluene, which were subjected to optical spectroscopic analyses without purification.

CdSe NCs were also synthesized using purified Cd precursors prepared from the TDPA-and-TOPO protocol (with 200-mg DOPO or DOPA). The purified Cd precursors (260–285 mg, see below) were combined with purified TOPO (3.80 g, 9.83 mmol) in a 50-mL Schlenk reaction tube and degassed under vacuum (0.1–0.2 torr) at 150 °C for 1 h. The tube was back-filled with N<sub>2</sub> and switched to a 275 °C salt bath. The NC synthesis then followed the same procedure as above.

### Synthesis of CdSe NCs using the OA-and-TOPO protocol

The procedure was adapted from Peng and coworkers.<sup>11,14</sup> Briefly, CdO (51 mg, 0.397 mmol), OA (448 mg, 0.801 mmol), and DOPA (0–200 mg, 0–0.689 mmol) or DOPO (0–200 mg, 0–0.729 mmol) were loaded into a 50-mL Schlenk reaction tube. The mixture was degassed under vacuum (0.1–0.2 torr) at room temperature for 10 min, back-filled with N<sub>2</sub>, and then inserted into a 250 °C salt bath to achieve a clear and colorless solution (8 min). After degassing under vacuum (0.1–0.2 torr) at ~100 °C for 10 min and back-filling with N<sub>2</sub>, the tube was loaded with purified TOPO (3.80 g, 9.83 mmol). After further degassing under vacuum (0.1–0.2 torr) at 150 °C for 1 h and back-filling with N<sub>2</sub>, the tube was switched to a 275 °C salt bath in which the temperature was allowed to equilibrate for 5 min. The NC synthesis then followed the same procedure as in the TDPA-and-TOPO/ODE/PDE protocol above.

### Characterization of Cd precursors

The clear and colorless Cd-precursor solution from the TDPA-and-TOPO/ODE protocol after the second degassing process was allowed to cool to ~100 °C for the subsequent purification in air. (Lower temperatures were found ineffective to remove free DOPA, as indicated by the presence of a sharp resonance at ~57 ppm in the <sup>31</sup>P NMR spectra.)

Acetone was added to cause a white cloudy suspension. A white precipitate was separated by centrifugation, which was washed three additional times by acetone, and finally dried under dynamic vacuum for 1 h to yield a white gel-like solid (260–285 mg, referred to as purified Cd precursor). The purified Cd precursor (~100 mg) was dissolved in  $d_8$ -toluene (1 mL) at ~80–100 °C under N<sub>2</sub> and then transferred to a N<sub>2</sub>-filled, septum capped NMR tube. After initial <sup>31</sup>P NMR-spectral acquisition, (Me<sub>3</sub>Si)<sub>2</sub>S (~60 µL, ~0.28 mmol) was added via syringe to the NMR tube,<sup>54</sup> with shaking to ensure thorough mixing. <sup>31</sup>P NMR spectra were acquired after 24 h.

The supernatant isolated from the first centrifugation process was evacuated under dynamic vacuum to remove volatiles. A small quantity of the product (~0.5 g) was then dissolved in  $d_8$ -toluene for <sup>31</sup>P NMR analysis.

### Synthesis of DOP

DOPO (5.0 g, 18.2 mmol) dissolved in dried THF (~20 mL) was added over 15 min to a N<sub>2</sub>-protected, well-stirred suspension of LiAlH<sub>4</sub> (1.0 g, 26.4 mmol) in dried THF (~20 mL) at ~0 °C. After the mixture was kept stirring for 1.5 h at room temperature under N<sub>2</sub>, degassed water (2 mL) was slowly added and the mixture was stirred for 10 min. After filtration under N<sub>2</sub>, the filtrate was introduced into a flask containing magnesium sulfate and stirred for 10 min. The mixture was then filtered (under N<sub>2</sub>) and the filtrate was evacuated (~50 °C, 0.5 Torr) to remove volatiles. Subsequent distillation (95–105 °C, 0.5 Torr) yielded a colorless liquid (3.0 g, 11.6 mmol, 64%). <sup>1</sup>H NMR ( $\delta$ , ppm,  $d_8$ -toluene, 25 °C): 3.06 (d,  $^1J_{P-H}$  = 189 Hz, 1 H), 1.40–1.70 (m, 8 H), 1.10–1.40 (m, 20 H), 0.89 (t,  $J$  = 7 Hz, 6 H) (Figure S1 in the Supporting Information). <sup>13</sup>C{<sup>1</sup>H} NMR ( $\delta$ , ppm,  $d_8$ -toluene, 25 °C): 32.32, 31.54 (d,  $^1J_{P-C}$  = 9 Hz), 29.80, 29.73, 28.89 (d,  $^1J_{P-C}$  = 10 Hz), 23.08, 20.98 (d,  $^1J_{P-C}$  = 11 Hz), 14.01 (Figure S1). <sup>31</sup>P NMR ( $\delta$ , ppm,  $d_8$ -toluene, 25 °C): 68.90 (d,  $^1J_{P-H}$  = 189 Hz, Figure S14). High-resolution (HR) MS (m/z): ([DOP + H]<sup>+</sup>), calcd. for C<sub>16</sub>H<sub>36</sub>P, 259.2549; found, 259.2556 (Figure S1).

### NMR Methods

<sup>1</sup>H and <sup>13</sup>C{<sup>1</sup>H} NMR spectra were recorded at 300 MHz and 75 MHz, respectively on a Varian Unity Plus-300 spectrometer in  $d_8$ -toluene or CDCl<sub>3</sub>, and the chemical shifts (in ppm) were referenced to TMS. <sup>31</sup>P NMR spectra were acquired at 121.4 MHz at a relaxation delay of ≥5 s in  $d_8$ -toluene, and the chemical shifts reported (in ppm) relative to external 85% phosphoric acid ( $\delta$  = 0 ppm).

The <sup>31</sup>P NMR spectra of the reaction mixtures of the CdSe NCs were acquired under N<sub>2</sub> protection. A septum-sealed NMR tube was evacuated (0.1–0.2 torr) through a needle insertion at room temperature for 1 min and was backfilled with N<sub>2</sub>. This process was repeated three additional times and the NMR tube was back-filled with N<sub>2</sub> and then loaded with  $d_8$ -toluene (0.5 mL) via syringe. Into the tube was injected via syringe the reaction mixture (~0.4 mL) taken at 40 s or 30 min of the reaction, with shaking to ensure thorough mixing. <sup>31</sup>P NMR was acquired at room temperature within 24 h.

The relative changes (mol %) of TOPSe (or percentages of TOPSe disappeared) in the reaction mixtures at 40 s or 30 min with respect to at 0 min (when reactants were mixed but no reactions occurred) and the conversion of DOPA to DOPA anhydride were estimated below. The initial (at 0 min) molar concentrations of TOPSe ([A]) in the reaction mixtures were calculated based on the peak integral in the <sup>31</sup>P{<sup>1</sup>H} NMR spectrum of TOPSe and the total amount of the P-containing compounds (TOP, TOPSe, DOPO/DOPA, TDPA, and TOPO) employed, where the impurities in TOP were assumed to have the same molecular weight as TOP. The measurement errors were approximately ± 2–5%. The molar

concentrations of TOPSe ([B]), DOPA ([C]), and DOPA anhydride ([D]) at 40 s or 30 min of the reactions were estimated from peak integrals in the  $^{31}\text{P}\{\text{H}\}$  NMR spectra, where the amounts of DOP (equal to the amounts of DOPA as DOP and DOPA are the two products from a disproportionation reaction of DOPO, see Results) removed via the second degassing were included in the calculation to conserve the same total amounts of the P-containing compounds for consistency. The errors were approximately  $\pm 5\text{--}10\%$ . The percentage (mol %) of TOPSe disappeared (at 40 s or 30 min) with respect to at 0 min were thus calculated as  $([\text{A}]-[\text{B}])/[\text{A}]$ . The conversion (mol %) of DOPA to DOPA anhydride were measured as  $[\text{D}]/([\text{C}]+[\text{D}])$ .

## Results

### Morphology control and growth kinetics of CdSe NCs

The sizes and morphologies of CdSe NCs (using the TDPA-and-TOPO protocol; see Experimental) differed significantly with or without DOPA or DOPO added, as shown in Figure 1. Short QRs were prepared in the absence of additives (control, Figure 1a). Longer QRs were generated in the presence of DOPA, and the QR length increased while the diameter remained nearly unchanged as more DOPA was employed (Figure 1b-d). In contrast, near-spherical QDs were produced with the use of DOPO and became smaller as more DOPO was applied (Figure 1f-h). We note that the source of TOP also affected CdSe-NC synthesis. For instance, use of higher-purity (97%) TOP resulted in the growth of longer QRs (Figure 1e). The reason will be given later in this section. TEM images for specimens collected at earlier reaction times indicated the same shapes (QD vs. QR) but smaller sizes (Figure S4, Supporting Information). Representative high-resolution TEM (HRTEM) images showed that the CdSe NCs exhibited the wurtzite (WZ) structure (Figure 1), which was confirmed by their X-ray powder-diffraction (XRD) patterns (Figure S5).

Significant differences in the nucleation kinetics of CdSe NCs were observed with the use of DOPA or DOPO. The solution-color change (from colorless to yellow) was fast with DOPO added (0–20 s) and near instantaneous for 100- or 200-mg DOPO, while it was slow for the control ( $\sim 50$  s) and slower with DOPA added (50–70 s). This indicated fast nucleation events when using DOPO and slow ones when using DOPA.

The differences in the nucleation and growth kinetics of CdSe NCs were also monitored by extinction and photoluminescence (PL) spectroscopies (Figures 2 and S6). The QDs (with DOPO) appeared at earlier times than did the QRs (with DOPA, Figure 2a). A size-focusing event was observed at 2–3 min when the QDs exhibited the narrowest full-width-at-half-maximums (fwhms, 0.10–0.11 eV, Figure 2b). The broader fwhms (0.12–0.15 eV) with increasing time after 3 min and the slow and steady growth rates (Figure 2a) indicated that an Ostwald ripening process was actively involved. In the presence of DOPA, the QR fwhms quickly decreased with time to  $\sim 0.08$  eV and remained at this value till the end of the reaction, which is the result of the absence of Ostwald ripening as indicated by the continuing growth in both radial and axial dimensions and the near monodispersities maintained (Figure S7). The PL quantum yields (QYs) decreased with time in the presence of DOPA, while stayed surprisingly unchanged with the use of DOPO (Figure 2c). We observed similar nucleation and growth kinetics and morphology control when TOPO was replaced by ODE or PDE (see Figure S8 for details).

Using the OA-and-TOPO protocol, however, the morphologies of NCs were primarily QDs of pseudo-spherical shape, regardless of DOPA or DOPO added (Figure 3). The QDs prepared with DOPO were smaller than the control, whereas those prepared with DOPA were larger than the control and had broad diameter distributions. Representative HRTEM images of the prolate QDs showed the presence of stacking faults and zinc-blende (ZB)/WZ

phase admixtures along their long axes (ZB [111] and WZ [001]), in addition to some QDs of pure WZ structure (Figure 3). The existence of stacking faults and ZB domains was confirmed by the weakening (102) and (103) reflections in the XRD patterns (Figure S9).

Relatively faster nucleation kinetics were observed in the presence of OA than TDPA. The solution changed instantly from colorless to red for the control and with the use of DOPO (0–2 s), and took up to 20 s to change yellow and up to 50 s to change red in the presence of DOPA. Despite the initial slow kinetics when using DOPA, fast kinetics were achieved after 50 s and the overall kinetics were comparable to the control and to those of using DOPO (Figure S10). In addition, two peaks or high-energy shoulders in the PL spectra were observed over the period of first 3 min that disappeared with an outcome of spectral broadening at later times. This was a second nucleation event, resulting in the broadening of the size distributions as observed above.

Although the growth kinetics (Figure 4a) were consistent with those of using the TDPA-and-TOPO protocol (Figure 2a), the fwhms showed an opposite trend: broadening (0.10–0.13 eV) by using DOPA vs. narrowing (0.08–0.10 eV) by using DOPO (Figure 4b). Ostwald ripening might not exist for QDs grown in the presence of DOPA as indicated by the decreasing fwhms at later growth times. Most of the kinetic runs exhibited ‘bright points’<sup>11</sup> and the PL QYs were higher when using DOPO than DOPA (Figure 4c). In addition, the PL QYs decreased with more DOPA, but increased with more DOPO.

### **<sup>31</sup>P NMR spectroscopic analyses of reaction mixtures of CdSe NCs**

We next sought to determine via <sup>31</sup>P NMR what had changed in the reaction mixtures that resulted in such different outcomes in the morphology control. The <sup>31</sup>P NMR spectra collected for the reaction mixtures (using the TDPA-and-TOPO protocol) at 40 s and 30 min are shown in Figure 5. The obvious difference between the control (Figure 5a,b) and those of using DOPA (Figure 5c,d) is the presence of the DOPA peak (~48 ppm). Surprisingly, we did not observe DOPO (~32 ppm) but DOPO in the reaction mixtures using DOPO (Figure 5e,f). Although differences were evident in the mixtures of using DOPA (Figure 5c,d) and DOPO (Figure 5e,f), we argue below that they are not likely the cause for the different morphology control achieved.

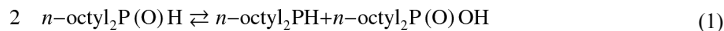
One of the major differences was the lower concentration of DOPA present in the reaction mixtures using DOPO (Figure 5e,f). However, the presence of DOPA with either small or large amounts should have resulted in the same synthetic outcome for both: the growth of QRs (although their lengths may vary. See Figure 1b,c), simply suggesting it is not this difference that caused the different morphologies. This further implied that DOPA might not play the same role in the morphology control in both conditions.

Another difference is the larger amount of DOPA anhydride (54 ppm) present when using DOPO. As mentioned in the Introduction, if an acid was incorporated into the Cd precursor and subsequently involved in the precursor conversion, its corresponding acid anhydride should be produced. The results shown here thus indicated that a much larger amount of DOPA was involved in the precursor conversion when using DOPO than using DOPA. The results presented above are confusing, but suggest that a link existed between the conversion yield of DOPA into DOPA anhydride and the morphology control of CdSe NCs. We observed similar results when TOPO was replaced by ODE or PDE (Figure S12).

When using the OA-and-TOPO protocol, different from above, DOPA was incorporated to form the Cd(di-*n*-octylphosphinate)<sub>x</sub>(oleate)<sub>2-x</sub> complexes (Figure S13).<sup>42</sup> In addition, significant amounts of DOPA anhydride appeared in both reactions of using DOPO or

DOPA, although DOPA anhydride was present in a smaller amount initially (at 40 s) when DOPA was used.

To understand the chemical transformation of DOPO during the precursor preparation, we heated DOPO under N<sub>2</sub> at 320 °C in a NMR tube with no degassing subsequently applied. Although a small amount of DOPO still remained, the majority of it had been converted into DOPA (55 ppm) and DOP (-69 ppm,  $J_{P-H} = 189$  Hz) with a ~1:1 molar ratio (Figure S14), in a typical disproportionation reaction (eq 1). Disproportionation reactions of primary and secondary phosphine oxides have been observed previously.<sup>39,57,58</sup> The assignments of DOPA and DOP were verified by adding authentic DOPA and DOP to the NMR tube, where an increase of the expected peaks was observed and no other peaks were noted. DOP was removed at 150 °C in the second degassing process when using TOPO as the solvent (see below), but still remained a small amount when using ODE or PDE as the solvent (Figures S11g and S12e,f).



In recognition of recently proposed reactions between TOP and TDPA in the synthesis of CdSe QRs<sup>52</sup> and in response to a reviewer's recommendation, we considered the impact of possible reaction products between TOP/DOPO and TDPA on the growth of CdSe NCs. Heating a mixture of TOP/DOPO and TDPA (Figures S15 and S16) under our conditions, however, did not result in detectable amounts of mono-*n*-tetradecylphosphinic acid, mono-*n*-tetradecylphosphine oxide, or mono-*n*-tetradecylphosphine as previously suggested,<sup>52</sup> but significant amounts of TDPA anhydride (a condensation product of TDPA) and DOPA and DOP (the disproportionation products of DOPO). The morphology control of our CdSe NCs in this study is thus not associated with the proposed reactions.<sup>52</sup>

As QDs were grown in both TOPO and ODE/PDE when using OA, we will focus in the next two sections on the NC syntheses using the TDPA-and-TOPO protocol. We contribute additional effort to identify what really caused the difference in the nucleation and growth kinetics and morphology control.

### Characterization of NC surface ligands

We first analyzed the surface ligands on the NCs with the hope of finding some differences. The <sup>31</sup>P NMR spectra of the recovered ligands were consistent with the previously reported results<sup>46,54,59</sup> that TDPA and TDPA anhydride were on the NC surface (Figure S17). Surprisingly, no DOPA was detected in the case of using DOPA or DOPO within the NMR-detection limit. The ratio of TDPA and TDPA anhydride varied among the control and those of using DOPA and DOPO, which was attributed to the varying degrees of Cd-precursor conversions<sup>54</sup> and the preparation history of the Cd precursors (see below).

The mass spectra of the recovered ligands showed the presence of TDPA, DOPA, and TOPO; however, the amount of TDPA was two orders of magnitude higher than DOPA and TOPO (Figure S18). The results established that even though a large amount of DOPA (DOPA:TDPA = 0.86) was employed in the NC synthesis, it was present in a very insignificant amount on the surface of the NCs. This implied that the anisotropic growth of QRs by using DOPA was unlikely a result of a variation in the binding affinity of DOPA on the different NC facets as discussed in the introduction, which was further supported by the fact that the presence of DOPA (converted from DOPO) did not result in the growth of QRs, but QDs.

### Cd precursors

A possible difference was imagined to be the Cd precursors prepared using DOPA and DOPO. After the second degassing, the precursor solutions were cooled to approximately 100 °C and acetone was added to precipitate white solids. The solid products (purified precursors) were characterized by  $^{31}\text{P}$  NMR spectroscopy and showed several broad resonances (Figure 6a,c), which became four sharp peaks as the purified precursors were treated with  $(\text{Me}_3\text{Si})_2\text{S}$ . One was derived from DOPA and the other three from TDPA and TDPA anhydride (Figure 6b,d), consistent with Figure S17 and the reported results.<sup>54,59</sup> The ratio between the DOPA derivative and the TDPA and TDPA anhydride derivatives was ~1:12 for the use of DOPO and ~1:13 for the use of DOPA. The incorporation of such a small amount of DOPA into the precursors was in match with the large amount of free DOPA left in the supernatants (see below), consistent with the lower stability and higher lability of the DOPA-derived Cd-di-*n*-octylphosphinate complexes as compared to the TDPA-derived Cd-*n*-tetradecylphosphonate complexes.<sup>42</sup> A second difference was observed in the ratio of the TDPA derivative and TDPA-anhydride derivative, which is higher for the precursor made in the presence of DOPA (1:4.7) than that (1:15.6) with the use of DOPO, consistent with the results for the surface ligands discussed above (Figure S17).

The TDPA anhydride in the Cd precursors was formed primarily from the process of dissolving CdO at high temperatures. Subsequent aging (where no degassing was applied after CdO dissolution) at room temperature under  $\text{N}_2$  significantly reduced the amount of TDPA anhydride (Figure S19). The results thus suggested that the preparation history (i.e., heating/dissolution time employed, with or without degassing after CdO dissolution, with or without aging) of the Cd precursors markedly changed the amount of TDPA anhydride present, which might explain the difference observed in the synthesis of CdSe QRs using freshly made or aged Cd-*n*-tetradecylphosphonate precursors.<sup>13</sup> In addition, the presence of DOPA and DOPO also caused differences (see above), a detailed reasoning of which, however, is beyond the scope of this paper.

We next determined whether it was the differences observed above that resulted in the growth of QRs or QDs by using DOPA or DOPO, respectively. We synthesized NCs by directly employing the two purified Cd precursors and TOPO to check whether the QDs and QRs could be reproduced. The two synthetic results, however, were similar in terms of shape control, both generating QRs with small variations in diameter and length (Figure 7). In addition, both spectroscopic data followed the similar trends (Figure S20). The experiments therefore established that the answer was not in the purified precursors.

The last possibility was thus expected to be in the supernatants. We observed a clear difference in the  $^{31}\text{P}$  NMR spectra of the two supernatants that a small amount of DOPO still remained with the use of DOPO (Figure 8b,c,e). This suggested that the disproportionation reaction of DOPO into DOPA and DOP had not gone to a completion over the course of Cd precursor preparation, consistent with the observation above of heating DOPO alone in a NMR tube (see Figure S14). This disproportionation reaction was continued in the NC synthesis, as confirmed by the appearance of DOP after the crude precursor mixture was heated at the reaction temperature (Figure 8a,f). The ultimate difference between the two crude precursors then became DOP. Was DOP responsible for the difference in the NC-morphology control observed?

To answer this question, we conducted an experiment by adding a small amount of independently synthesized DOP (22 mg/0.085 mmol, see Experimental) to the TOPSe solution, and injecting this solution into the Cd-precursor solution prepared without DOPA or DOPO. QDs were produced as expected (Figure 9a) and the spectroscopic data closely followed those of using 200-mg DOPO (Figure S21). Further more, when this DOP-

containing TOPSe solution was injected into the Cd-precursor solution prepared with 200-mg DOPA, QDs were also generated (Figure 9b), constituting a contrast to the growth of QRs where no DOP or DOPO coexisted with DOPA (see Figure 1d). And noteworthy the spectroscopic data closely followed the trends of those using 200-mg DOPO (Figure S21). This latter experiment thus at many aspects reproduced the result of using 200-mg DOPO and indicated a negligible role of DOPA in the NC-morphology control when DOP was present. DOP was therefore established to be responsible for QD growth.

We next estimated the amount of residual DOP in the actual synthesis with the use of 200-mg DOPO by measuring the amount of remaining DOPO after the second degassing process (Figure 8b). (The spectrum was transformed with 1-Hz line broadening, allowing the TOPO and DOPA resonances to be resolved.) The integrated peak area of DOPO (0.80) was compared to that of TOPO (100.00, 9.83 mmol) and the amount of DOPO was thus  $0.0080 * 9.83 = 0.079$  mmol. Since in the synthesis there coexisted the disproportionation of DOPO into DOP and the subsequent conversion of DOP (via DOPSe) into DOPO in the formation of CdSe nutrients (Scheme 1) and *vice versa*, the actual amount of DOP involved was estimated to be 0.079 mmol according to eq 2. The nucleation and growth kinetics of the CdSe NCs (Figure S20a) and the precursor-conversion kinetics (see the next section) with the use of 200-mg DOPO were thus comparable to those of NCs synthesized using independently synthesized DOP (0.085 mmol) shown above.

$$DOP = 0.079 \lim_{n \rightarrow \infty} \sum_{n=1}^{n=\infty} \frac{1}{2^n} \approx 0.079 \text{ mmol} \quad (2)$$

As DOP may be present with varying amounts in commercial TOP,<sup>37,39,41</sup> irreproducibility in the size and shape was thus expected in the CdSe-NC syntheses when different batches of TOP were employed. We found this is true in the two control experiments of using 90% (Figure 1a) and 97% TOP (Figure 1e), where longer QRs were grown using 97% TOP. <sup>31</sup>P NMR spectroscopy indicated that ~0.07 mol % of DOP was present in 90% TOP, whereas no DOP was detected in 97% TOP within the NMR-detection limit (Figure S22). The result is consistent with the observations discussed above that the isotropic growth of CdSe NCs (QDs) was favored in the presence of DOP.

### Precursor-conversion kinetics

We next determined the precursor-conversion kinetics that were presumably linked to the morphology control conferred by DOP or DOPA. We calculated the TOPSe conversions (percentages of TOPSe disappeared) based on the changes in the integrated peak-area of TOPSe in the <sup>31</sup>P NMR spectra of the reaction mixtures collected at 40 s and 30 min with respect to 0 min (see the Experimental Section for details). The results are shown in Figure 10. The data at 40 s are presented as dotted traces and those at 30 min as solid traces. The TOPSe conversions at 40 s increased in the order of using DOPA, DOPO, and DOP and were higher in the presence of OA than in the presence of TDPA. Considering that the precursor conversion was equal to the yield of crystalline CdSe and the initial precursor-conversion rate was proportional to the final number of nuclei,<sup>36</sup> we approximated the TOPSe conversion rates at 40 s to be the initial precursor-conversion rates. The number of nuclei generated increased in the order of using DOPA, DOPO, and DOP and was higher in the presence of OA than in the presence of TDPA (dotted traces, Figure 10a). The increasing number of nuclei with the use of more DOPO (blue and red dotted traces) was evident as a result of the presence of more DOP from a disproportionation reaction of DOPO. DOPA played a negligible role in the nucleation when DOP was added (olive dotted trace), whereas it decreased the number of nuclei, when DOP was absent (pink and black dotted traces).

We obtained the information about the growth kinetics by comparing the difference of TOPSe conversions at 40 s (dotted traces) and 30 min (solid traces), since this difference could be considered as the actual amount of nutrients consumed in the NC growth after nucleation. This decreased in the order of using DOPA, DOPO, and DOP. It, combining the increasing number of nuclei generated, accommodated the greatest volume growth for a NC when using DOPA, and the smallest one when using DOP, consistent with the large QRs and small QDs resulted, respectively (Figures 1d,h, 3d,g, and 9). In the presence of DOP, the majority of the nutrients were consumed at the beginning of the growth, as indicated by the fast NC size increase over the first 5 min and the later slow size increase (Figure S21a). In addition, high overall TOPSe conversions resulted (~50%, olive solid trace, Figure 10a), consistent with the high NC yields in the presence of DOP or diphenylphosphine as observed by Bawendi, Krauss, and Klimov and coworkers.<sup>37,39,41</sup> The highest TOPSe conversions (~72%) were achieved with the use of OA and DOPO (blue traces). Since the Cd precursor was the limiting reagent in the initial reaction solutions (ratio of Cd precursor to TOPSe = 0.78:1), the Cd-precursor conversions had reached ~72%/0.78 = 92%, thus near completion.

We gathered additional information on the precursor-conversion kinetics by monitoring the conversion of DOPA into DOPA anhydride at 30 min of the reactions (Figure 10b). This conversion was directly linked to DOPA that was involved in the precursor conversion, accounting for only DOPA that was incorporated into the Cd precursors. A small percentage (<9%) of DOPA was incorporated into the Cd precursors when using the TDPA-and-TOPO protocol (see above and Figure 6), whereas a large percentage (~80%) was incorporated when using OA-and-TOPO protocol.<sup>42</sup> As expected, the yield of DOPA anhydride was higher in the presence of OA than in the presence of TDPA. In addition, it was higher when using DOPO than using DOPA, and increased from near 0 to 4% when a small amount of DOP was added (in the presence of DOPA and TDPA, olive triangle, Figure 10b). The results were consistent with the TOPSe conversions observed above that high Se/Cd precursor conversions were involved when OA, DOPO, or DOP was employed. Furthermore, the yield of DOPA anhydride ( $\leq 8\%$  for using TDPA and  $\sim 80\%$  for using OA, red and blue solid traces, respectively) was approximately equal to the percentage of DOPA incorporated into the Cd precursors when using DOPO, suggesting an unselective role of DOPSe toward binding to the Cd precursors and the subsequent P=Se bond cleavage. The significantly lower yield of DOPA anhydride ( $\leq 1\%$  for using TDPA and  $\sim 50\%$  for using OA, black and pink solid traces, respectively) with the use of DOPA suggested that the steric hindrance from both DOPA and TOPSe should be taken into account.

## Discussion

At least four mechanisms have been suggested for achieving anisotropic growth of colloidal semiconductor NCs. First, the solution–liquid–solid (SLS) growth mechanism has been established, where metallic nanoparticles are employed as the seeds to catalyze the growth of QW and QRs.<sup>42,60–62</sup> Second, the oriented-attachment mechanism has been identified, where the key steps involved are the alignment and subsequent attachment of small NCs (or building blocks) along specific lattice planes, driven by the existence of a dipole moment in the NCs and by the total surface-energy reduction. The primary NCs fuse epitaxially (along a specific axis) to form necklace-like anisotropic structures, as observed in the intermediate stage.<sup>63,64</sup> Our results apparently do not follow these two mechanisms.

Third, a ligand-directed anisotropic growth has been proposed, where variations in binding energies/affinities of ligands to different crystallographic facets control the relative growth rates of different facets, achieving the anisotropic growth of the NCs.<sup>3,19,29–32</sup> A typical example is WZ CdSe, which grows unidirectionally along the [001] direction in the presence

of alkylphosphonic acids to form QRs, as a result of the increased growth rate of the (001) facet due to the weaker binding of alkylphosphonic acids on this facet.<sup>19,29-32</sup>

Fourth, a ligand-modified precursor reactivity or nutrient activity has been proposed to control the morphology of the NCs.<sup>1,13,33-35</sup> The central point of this mechanism is the balance between nucleation and growth that is determined by the precursor reactivities or nutrient activities in the reaction systems. Growth of anisotropic shapes is favored under conditions having small numbers of nuclei and high concentrations of remaining nutrients in the solution, which are fulfilled by using precursors having low reactivities.<sup>1,13,33-35</sup> For example, alkylphosphonate ligands bind more strongly to Cd precursor complexes than do alkylcarboxylate ligands and thus decrease the reactivities of the precursors.<sup>13,21</sup> Consequently, Cd-alkylphosphonate complexes result in CdSe QR growth, whereas Cd-alkylcarboxylate complexes generate QDs.<sup>13,21,23,34</sup>

Both the third<sup>3,19,29-32</sup> and fourth<sup>1,13,33-35</sup> mechanisms require the presence of strongly binding ligands and high nutrient concentrations to maintain anisotropic growth, and both mechanisms may coexist in a reaction system.<sup>33,34</sup> Our results support the fourth mechanism. We achieved morphology control of NCs through the control of the precursor-conversion kinetics, and thereby the nucleation kinetics as shown above, which were determined by the precursor reactivities. Although the precursor reactivity was used on a quantitative basis, we found that we could not precisely interpret the precursor-conversion kinetics by using the precursor reactivity alone in a system containing more than one precursor or additive, as the reactivity of a precursor (i.e., the Cd precursor) was significantly coupled with or dependent on that of another precursor (i.e., the Se precursor) (see below). We propose below that the morphology control of NCs that is governed by the precursor-conversion kinetics can be best understood at the microscopic (molecular) scale in terms of the reaction chemistry of the precursors and ligands.

Insights into the precursor-conversion kinetics were provided by the elucidations of the reaction mechanisms for the analogous syntheses of II–VI,<sup>36,38</sup> III–V,<sup>40</sup> and IV–VI<sup>37,39</sup> QDs. The syntheses were shown to follow the pathway outlined in Scheme 1, in which CdSe formation is presented as a specific example. The structural differences in R<sub>3</sub>PSe or Cd(OX)<sub>2</sub> have been shown to affect the precursor-conversion kinetics. For example, slower kinetics were observed using sterically hindered triisopropylphosphine selenide<sup>38</sup> and aryl substituted tertiary phosphine selenides,<sup>36</sup> whereas rapid kinetics were observed in the presence of a secondary phosphine selenide.<sup>37,39,41</sup> Cd-alkylphosphonate complexes exhibited slower kinetics than did Cd-alkylcarboxylate complexes.<sup>38,42</sup> DOPA-substituted {Cd[O<sub>2</sub>P(*n*-octyl)<sub>2</sub>]<sub>x</sub>[oleate]<sub>2-x</sub>}<sub>n</sub> complexes showed faster kinetics than Cd-alkylphosphonate complexes while slower kinetics than Cd-alkylcarboxylate complexes, due to the intermediate Lewis acidities, labilities, and stabilities that {Cd[O<sub>2</sub>P(*n*-octyl)<sub>2</sub>]<sub>x</sub>[oleate]<sub>2-x</sub>}<sub>n</sub> complexes exhibited.<sup>42</sup>

Our results of fast initial precursor-conversion kinetics by using DOP or the Cd-oleate complexes are thus consistent with the above observations. Interestingly, partial ligand substitution of Cd-oleate or Cd-*n*-tetradecylphosphonate complexes by (*n*-octyl)<sub>2</sub>PO<sub>2</sub><sup>-</sup> (see above) had little effects on the kinetics if DOP was present. We observed fast initial precursor-conversion kinetics even in the presence of large amounts of DOPA, demonstrating that DOPSe played a sole, predominating role in controlling the reaction kinetics as a result of its small steric hindrance or a possibly different mechanism involved in the P=Se bond cleavage for secondary phosphine selenides.<sup>39,65,66</sup> In this situation, the structures of Cd precursors had negligible effects on the kinetics. As a result, fast initial precursor-conversion kinetics generated a large number of nuclei,<sup>36</sup> and all these nuclei competed for the remaining CdSe nutrients generated in Scheme 1. This resulted in a rapid

decline of CdSe-nutrient concentration in solution, a situation that is a prerequisite for keeping the system in the isotropic (QD) growth regime.

The greater number of nuclei generated with the use of a larger amount of DOPO (or DOP) was further confirmed by the greater number of NCs at the end of the reaction (30 min) as shown in Figure 11a. The numbers of NCs with the use of DOPO were obtained as normalized ones (black squares) with respect to the control, and were estimated based on the NC sizes measured from the TEM images (see Figure 1) and the overall TOPSe conversions obtained (see Figure 10), based on the fact that the precursor conversion was equal to the yield of crystalline CdSe (see Table S1 and the associated text in the Supporting Information for detailed calculations).<sup>36</sup> Since changes in either the numbers of nuclei or TOPSe conversions can contribute to the changes in the NC sizes (or volumes), the specific contributions (red squares vs. blue squares, Figure 11a) were thus differentiated (see Table S1). The size/volume decreases with increasing amounts of DOPO (or DOP) were solely due to the increased numbers of QDs generated, as the small size/volume increases contributed from the increased TOPSe conversions (blue squares, Figure 11a) were entirely offset by the greater size/volume decreases contributed from the increased numbers of QDs generated (red squares, Figure 11a).

The structures of Cd precursors had strong effects on the precursor-conversion kinetics when TOPSe was used where DOP or DOPO was absent. Cd-oleate complexes had fast kinetics as discussed above. In contrast, Cd-*n*-tetradecylphosphonate complexes (the control) exhibited slow initial precursor-conversion kinetics, resulting in a small number of nuclei and a sufficiently high concentration of remaining CdSe nutrients in the solution. This favored the preferential growth along the [001] axis of the intrinsically anisotropic WZ CdSe to form QRs. Addition of DOPA into Cd-*n*-tetradecylphosphonate precursors resulted in slower kinetics (slower color change) and thus the expected longer CdSe QRs. Because partial ligand substitution of Cd-*n*-tetradecylphosphonate complexes by (*n*-octyl)<sub>2</sub>PO<sub>2</sub><sup>-</sup> could decrease the stability and increase the lability and Lewis acidity of the precursors as discussed above, greater kinetics should have been observed instead. Considering the corresponding lower yield of DOPA anhydride (black trace, Figure 10b) than that using DOPO (red trace, Figure 10b), we attribute such slower kinetics (slower color change) to the steric hindrance of DOPA and TOPSe as DOPA and TOPSe are more bulky than TDPA and DOPSe, respectively (see Scheme 1).

The growth of long QRs in the presence of excess TDPA and DOPA is also reminiscent of the well-documented increase in NC size with increasing acid concentration, due to the decreasing number of nuclei generated.<sup>23,36,41,43,67</sup> As shown in Figure 11b, the increase in the QR length in the presence of DOPA was only partially due to the smaller number of QRs generated (red squares), and a more significant contribution was from the increased overall TOPSe conversions, as observed at high DOPA concentrations (blue squares). These greater growth kinetics were consistent with the observed faster NC growth rates at higher concentrations of acids (i.e., TDPA, and OA).<sup>36,43</sup> In contrast, the growth kinetics (the differences between the red solid and dotted traces, Figure 10a; blue squares, Figure 11a) for QDs were nearly unchanged with increasing DOPA (converted from DOPO) concentrations when using more DOPO. This implied that different mechanisms were involved in the growth of QDs and QRs. Our observations were consistent with the predominant thermodynamic control in the QD growth, which was indicated by the presence of Ostwald ripening (Figure 2a,b), as discussed above. The greater growth kinetics of QRs at higher DOPA concentrations and lack of evident Ostwald ripening (Figure 2a,b) suggested the predominant kinetic control in the QR growth.

In the case of adding DOPA into the Cd-oleate precursors where (*n*-octyl) PO<sub>2</sub><sup>-</sup> was incorporated to form {Cd[O<sub>2</sub>P(*n*-octyl)<sub>2</sub>]<sub>x</sub>[oleate]<sub>2-x</sub>}<sub>n</sub> (where x was estimated to be ~1.4 in the presence of 200-mg DOPA,<sup>42</sup> and DOP or DOPO was absent), we observed two nucleation events within the first 3 min of the reactions (Figure S10). We attributed the fast nucleation primarily to the Cd-oleate component because of the fast precursor-conversion kinetics observed for Cd-oleate complexes, and the slower one to the Cd-di-*n*-octylphosphinate component, as evident by the low conversion of DOPA to DOPA anhydride (~4%, Figure S13c) at 40 s that accounted for ~40% of the total Cd-precursor conversion (Figure 10a). This was supported by the higher stability and lower lability and Lewis acidity of Cd-di-*n*-octylphosphinate complexes than that of Cd-oleate complexes. In addition, effects of high steric hindrance from DOPA and TOPSe existed as evidenced by the lower DOPA-anhydride conversion when using DOPA than using DOPO (pink trace vs. blue trace, Figure 10b). The two nucleation events and their associated fast precursor-conversion kinetics (but relatively slower than the control, see the Results) resulted in the growth of QDs having broad diameter distributions. In addition, the smaller numbers of nuclei using DOPA than using DOPO (pink vs. blue dotted traces, Figure 10a) led to larger QDs.

## Conclusion

We have identified that precursor-conversion kinetics, which were determined by the precursors, quantitatively determined the nucleation and growth kinetics and thus the morphologies of NCs. The growth of QDs was favored by fast nucleation kinetics as a result of fast initial precursor-conversion kinetics, under conditions of using secondary phosphine selenides (i.e., DOPSe) or more Lewis-acidic and labile precursors (i.e., Cd-alkylcarboxylate complexes). Slow nucleation kinetics due to slow initial precursor-conversion kinetics favored the growth of QRs, in the case of using more sterically hindered TOPSe and less Lewis-acidic and labile Cd-alkylphosphonate precursors. However, fast post-nucleation precursor-conversion kinetics (the differences between the black dotted and solid traces, Figure 10a) should be maintained to achieve the fast growth of QRs, which was required to be under kinetic control. Therefore, the origin of the anisotropic morphology proposed in the first QR paper turns out to be correct.<sup>1</sup> This precursor-conversion-mediated morphology control should be applicable to colloidal semiconductor NCs that have intrinsically anisotropic crystal (i.e., WZ) structures. Our findings provide further understanding of the complex chemistry associated with nucleation and growth of semiconductor NCs, which may allow more rational shape-controlled syntheses of semiconductor NCs.

## Supplementary Material

Refer to Web version on PubMed Central for supplementary material.

## Acknowledgments

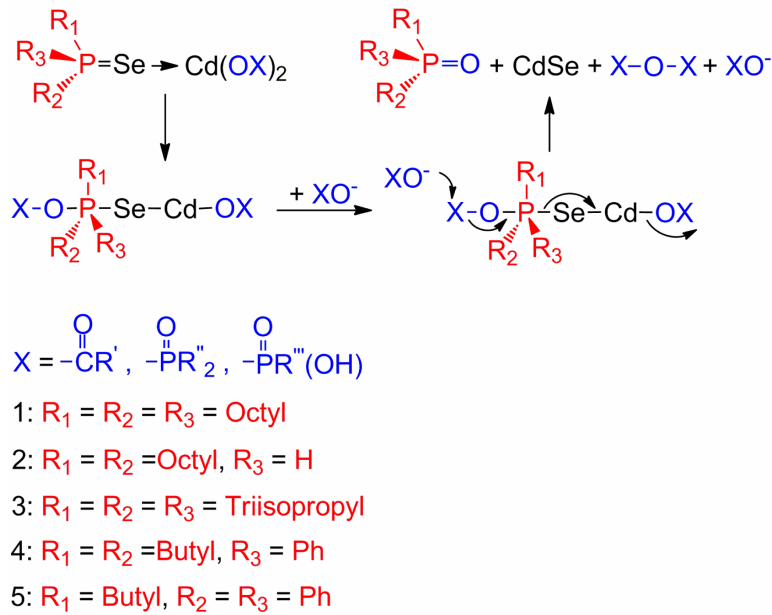
We thank Mr. Xing Yang (Washington U) for helpful discussions. This work was supported by NSF (CHE-1012898). Mass spec-trometry was provided by the Washington University Mass Spec-trometry Resource, an NIH Research Resource (Grant No. P41RR0954).

## REFERENCES

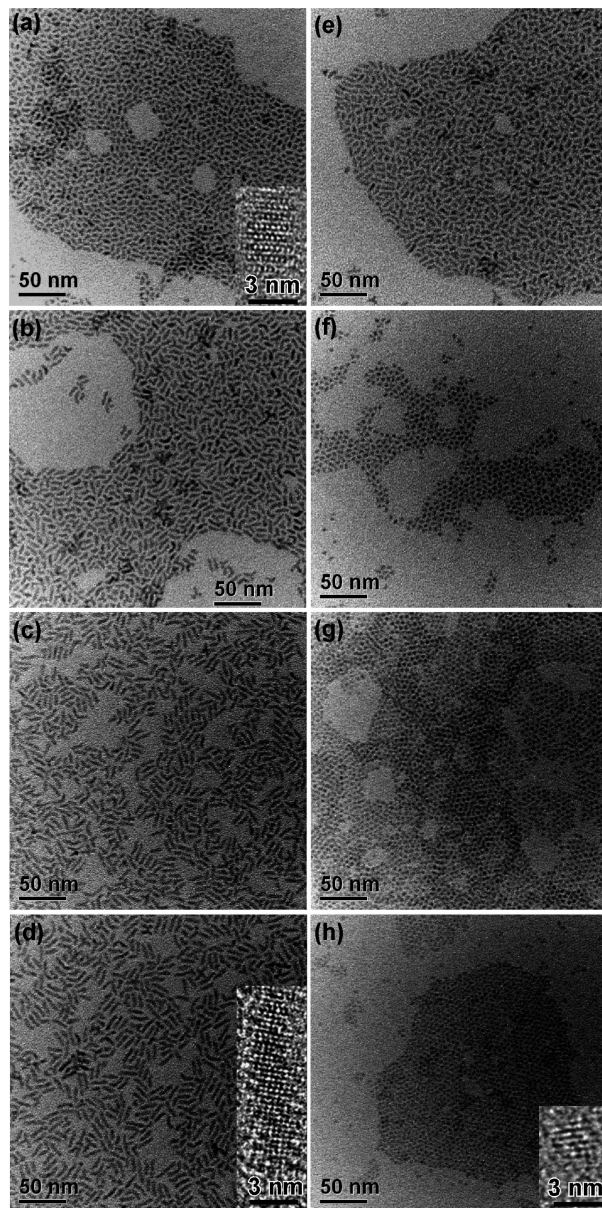
1. Peng XG, Manna L, Yang WD, Wickham J, Scher E, Kadavanich A, Alivisatos AP. *Nature*. 2000; 404:59–61. [PubMed: 10716439]
2. Milliron DJ, Hughes SM, Cui Y, Manna L, Li JB, Wang LW, Alivisatos AP. *Nature*. 2004; 430:190–195. [PubMed: 15241410]

3. Manna L, Milliron DJ, Meisel A, Scher EC, Alivisatos AP. *Nat. Mater.* 2003; 2:382–385. [PubMed: 12764357]
4. Talapin DV, Rogach AL, Kornowski A, Haase M, Weller H. *Nano Lett.* 2001; 1:207–211.
5. Talapin DV, Koeppe R, Gotzinger S, Kornowski A, Lupton JM, Rogach AL, Benson O, Feldmann J, Weller H. *Nano Lett.* 2003; 3:1677–1681.
6. Chan EM, Xu CX, Mao AW, Han G, Owen JS, Cohen BE, Milliron DJ. *Nano Lett.* 2010; 10:1874–1885. [PubMed: 20387807]
7. Mekis I, Talapin DV, Kornowski A, Haase M, Weller H. *J. Phys. Chem. B.* 2003; 107:7454–7462.
8. Micic OI, Curtis CJ, Jones KM, Sprague JR, Nozik AJ. *J. Phys. Chem.* 1994; 98:4966–4969.
9. Hines MA, Guyot-Sionnest P. *J. Phys. Chem.* 1996; 100:468–471.
10. Schwartz DA, Norberg NS, Nguyen QP, Parker JM, Gamelin DR. *J. Am. Chem. Soc.* 2003; 125:13205–13218. [PubMed: 14570496]
11. Qu LH, Peng XG. *J. Am. Chem. Soc.* 2002; 124:2049–2055. [PubMed: 11866620]
12. Pradhan N, Goorskey D, Thessing J, Peng XG. *J. Am. Chem. Soc.* 2005; 127:17586–17587. [PubMed: 16351071]
13. Peng ZA, Peng XG. *J. Am. Chem. Soc.* 2002; 124:3343–3353. [PubMed: 11916419]
14. Peng ZA, Peng XG. *J. Am. Chem. Soc.* 2001; 123:183–184. [PubMed: 11273619]
15. Peng XG, Wickham J, Alivisatos AP. *J. Am. Chem. Soc.* 1998; 120:5343–5344.
16. Murphy JE, Beard MC, Norman AG, Ahrenkiel SP, Johnson JC, Yu PR, Micic OI, Ellingson RJ, Nozik AJ. *J. Am. Chem. Soc.* 2006; 128:3241–3247. [PubMed: 16522105]
17. Mokari TL, Zhang MJ, Yang PD. *J. Am. Chem. Soc.* 2007; 129:9864–9865. [PubMed: 17658815]
18. Manna L, Scher EC, Li LS, Alivisatos AP. *J. Am. Chem. Soc.* 2002; 124:7136–7145. [PubMed: 12059239]
19. Manna L, Scher EC, Alivisatos AP. *J. Am. Chem. Soc.* 2000; 122:12700–12706.
20. Joo J, Na HB, Yu T, Yu JH, Kim YW, Wu FX, Zhang JZ, Hyeon T. *J. Am. Chem. Soc.* 2003; 125:11100–11105. [PubMed: 12952492]
21. Yu WW, Wang YA, Peng XG. *Chem. Mater.* 2003; 15:4300–4308.
22. Mokari T, Banin U. *Chem. Mater.* 2003; 15:3955–3960.
23. Yu WW, Peng XG. *Angew. Chem. Int. Ed.* 2002; 41:2368–2371.
24. Battaglia D, Li JJ, Wang YJ, Peng XG. *Angew. Chem. Int. Ed.* 2003; 42:5035–5039.
25. Yen BKH, Stott NE, Jensen KF, Bawendi MG. *Adv. Mater.* 2003; 15:1858–1862.
26. Kloper V, Osovsky R, Kolny-Olesiak J, Sashchiuk A, Lifshitz E. *J. Phys. Chem. C.* 2007; 111:10336–10341.
27. Yang YA, Wu HM, Williams KR, Cao YC. *Angew. Chem. Int. Ed.* 2005; 44:6712–6715.
28. Murray CB, Norris DJ, Bawendi MG. *J. Am. Chem. Soc.* 1993; 115:8706–8715.
29. Scher EC, Manna L, Alivisatos AP. *Philos. Trans. R. Soc. London, Ser. A.* 2003; 361:241–255.
30. Puzder A, Williamson AJ, Zaitseva N, Galli G, Manna L, Alivisatos AP. *Nano Lett.* 2004; 4:2361–2365.
31. Rempel JY, Trout BL, Bawendi MG, Jensen KF. *J. Phys. Chem. B.* 2006; 110:18007–18016. [PubMed: 16956292]
32. Manna L, Wang LW, Cingolani R, Alivisatos AP. *J. Phys. Chem. B.* 2005; 109:6183–6192. [PubMed: 16851684]
33. Peng XG, Thessing J. *Struct. Bonding.* 2005; 118:79–119.
34. Peng ZA, Peng XG. *J. Am. Chem. Soc.* 2001; 123:1389–1395.
35. Peng XG. *Adv. Mater.* 2003; 15:459–463.
36. Owen JS, Chan EM, Liu HT, Alivisatos AP. *J. Am. Chem. Soc.* 2010; 132:18206–18213. [PubMed: 21128655]
37. Steckel JS, Yen BKH, Oertel DC, Bawendi MG. *J. Am. Chem. Soc.* 2006; 128:13032–13033. [PubMed: 17017765]
38. Liu HT, Owen JS, Alivisatos AP. *J. Am. Chem. Soc.* 2007; 129:305–312. [PubMed: 17212409]

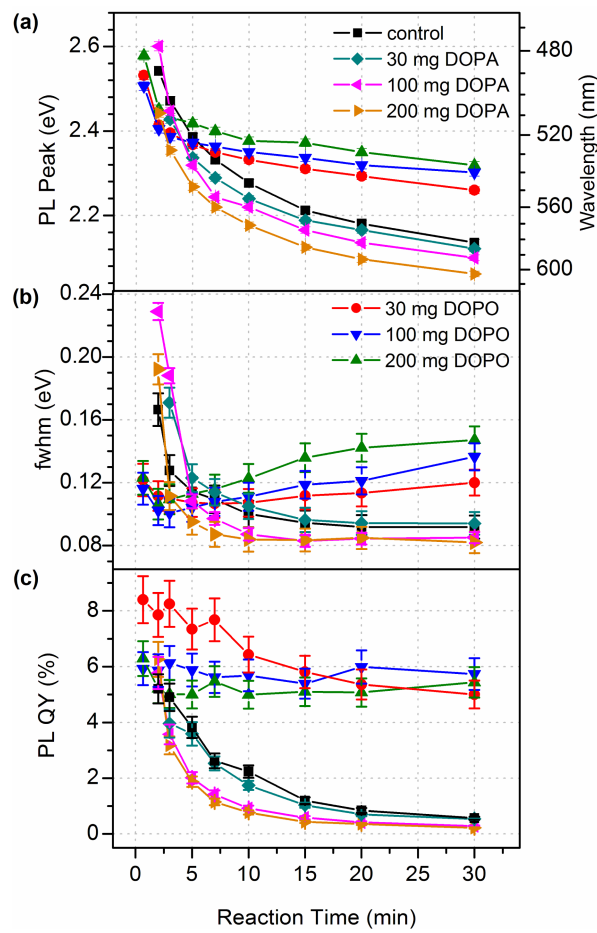
39. Evans CM, Evans ME, Krauss TD. *J. Am. Chem. Soc.* 2010; 132:10973–10975. [PubMed: 20698646]
40. Allen PM, Walker BJ, Bawendi MG. *Angew. Chem. Int. Ed.* 2010; 49:760–762.
41. Joo J, Pietryga JM, McGuire JA, Jeon SH, Williams DJ, Wang HL, Klimov VI. *J. Am. Chem. Soc.* 2009; 131:10620–10628. [PubMed: 19569687]
42. Wang F, Tang R, Kao JLF, Dingman SD, Buhro WE. *J. Am. Chem. Soc.* 2009; 131:4983–4994. [PubMed: 19296595]
43. Bullen CR, Mulvaney P. *Nano Lett.* 2004; 4:2303–2307.
44. Xie RG, Li Z, Peng XG. *J. Am. Chem. Soc.* 2009; 131:15457–15466. [PubMed: 19775131]
45. Rempel JY, Bawendi MG, Jensen KF. *J. Am. Chem. Soc.* 2009; 131:4479–4489. [PubMed: 19275244]
46. Morris-Cohen AJ, Donakowski MD, Knowles KE, Weiss EA. *J. Phys. Chem. C.* 2010; 114:897–906.
47. Kawa MM,H, Ioku A, Saita S, Okuyama K. *J. Nanopart. Res.* 2003; 5:81–85.
48. Kopping JTP, T. E. *J. Am. Chem. Soc.* 2008; 130:5689–5698.
49. Wang FD, Tang R, Buhro WE. *Nano Lett.* 2008; 8:3521–3524. [PubMed: 18754691]
50. Wolcott A, Fitzmorris RC, Muzaffery O, Zhang JZ. *Chem. Mater.* 2010; 22:2814–2821. [PubMed: 20473338]
51. Wang W, Banerjee S, Jia SG, Steigerwald ML, Herman IP. *Chem. Mater.* 2007; 19:2573–2580.
52. Jiang ZJ, Kelley DF. *ACS Nano.* 2010; 4:1561–1572. [PubMed: 20192241]
53. Kanaras AG, Sonnichsen C, Liu HT, Alivisatos AP. *Nano Lett.* 2005; 5:2164–2167. [PubMed: 16277446]
54. Owen JS, Park J, Trudeau PE, Alivisatos AP. *J. Am. Chem. Soc.* 2008; 130:12279–12281. [PubMed: 18722426]
55. Talapin DV, Nelson JH, Shevchenko EV, Aloni S, Sadtler B, Alivisatos AP. *Nano Lett.* 2007; 7:2951–2959. [PubMed: 17845068]
56. Li LS, Hu JT, Yang WD, Alivisatos AP. *Nano Lett.* 2001; 1:349–351.
57. Majewski P. *Synthesis-Stuttgart.* 1987:554–555.
58. Yakhvarov D, Caporali M, Gonsalvi L, Latypov S, Mirabello V, Rizvanov I, Sinyashin O, Stoppioni P, Peruzzini M. *Angew. Chem. Int. Ed.* 2011; 50:5370–5373.
59. Gomes R, Hassinen A, Szczygiel A, Zhao QA, Vantomme A, Martins JC, Hens Z. *J. Phys. Chem. Lett.* 2011; 2:145–152.
60. Wang FD, Buhro WE. *J. Am. Chem. Soc.* 2007; 129:14381–14387. [PubMed: 17967017]
61. Wang FD, Dong AG, Sun JW, Tang R, Yu H, Buhro WE. *Inorg. Chem.* 2006; 45:7511–7521. [PubMed: 16961336]
62. Kan S, Mokari T, Rothenberg E, Banin U. *Nat. Mater.* 2003; 2:155–158. [PubMed: 12612671]
63. Tang ZY, Kotov NA, Giersig M. *Science.* 2002; 297:237–240. [PubMed: 12114622]
64. Pacholski C, Kornowski A, Weller H. *Angew. Chem. Int. Ed.* 2002; 41:1188–1191.
65. García-Rodríguez R, Liu H. *J. Am. Chem. Soc.* 2012; 134:1400–1403. [PubMed: 22225464]
66. Cossairt BM, Owen JS. *Chem. Mater.* 2011; 23:3114–3119.
67. Urban JJ, Talapin DV, Shevchenko EV, Murray CB. *J. Am. Chem. Soc.* 2006; 128:3248–3255. [PubMed: 16522106]



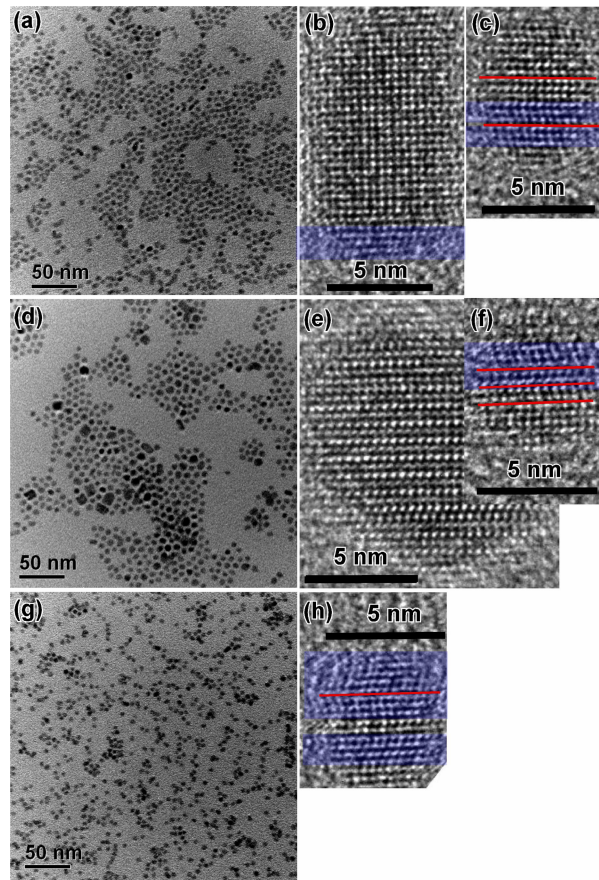
**Scheme 1.**  
Binding and Cleavage Mechanism of Phosphine Selenide.<sup>36-39,42</sup>

**Figure 1.**

Representative TEM images of CdSe NCs grown (30-min reaction time) using the TDPA-and-TOPO protocol: control (no DOPA or DOPO added, a and e), with DOPA (30 mg, 0.10 mmol, b; 100 mg, 0.34 mmol, c; 200 mg, 0.69 mmol, d), and with DOPO (30 mg, 0.11 mmol, f; 100 mg, 0.36 mmol, g; 200 mg, 0.73 mmol, h). 90% TOP was used, except for (e) for which 97% TOP was employed. The measured sizes (diameter ( $d$ )  $\times$  length ( $l$ ) or  $d \pm$  one standard deviation in  $d$  or  $l$  distribution) by TEM are: (a)  $3.6\text{ nm} (\pm 11\%) \times 5.7\text{ nm} (\pm 19\%)$ , (b)  $3.8\text{ nm} (\pm 11\%) \times 8.8\text{ nm} (\pm 24\%)$ , (c)  $3.9\text{ nm} (\pm 10\%) \times 12.2\text{ nm} (\pm 21\%)$ , (d)  $4.2\text{ nm} (\pm 10\%) \times 15.3\text{ nm} (\pm 18\%)$ , (e)  $3.9\text{ nm} (\pm 11\%) \times 7.2\text{ nm} (\pm 21\%)$ , (f)  $3.4\text{ nm} (\pm 15\%) \times 3.9\text{ nm} (\pm 18\%)$ , (g)  $3.3\text{ nm} (\pm 15\%)$ , and (h)  $3.0\text{ nm} (\pm 16\%)$ . Insets are the corresponding HRTEM images showing the WZ crystal structure.

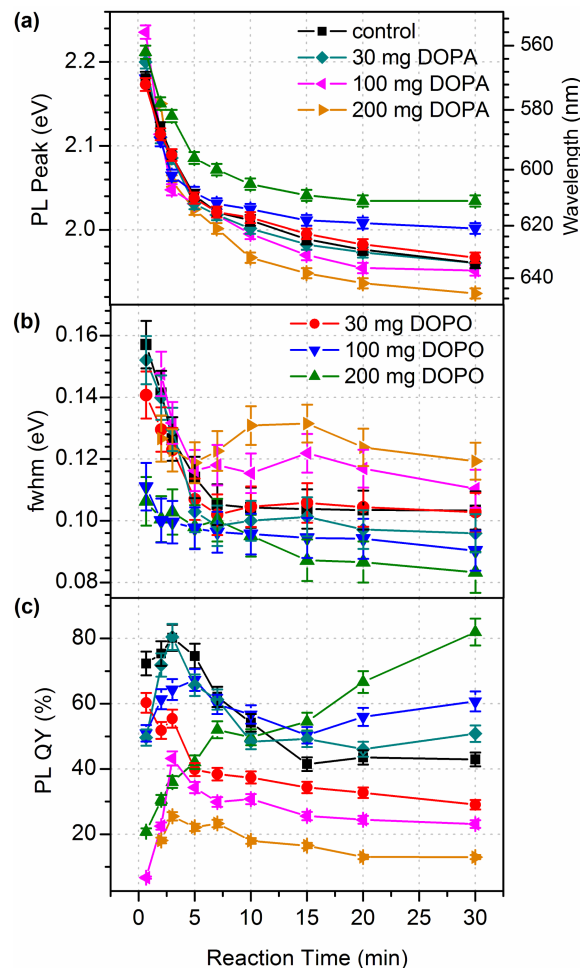
**Figure 2.**

Temporal evolution of PL peak position (a), PL fwhm (b), and PL QY (c) of CdSe NCs grown using the TDPA-and-TOPO protocol with or without the addition of DOPA or DOPO.

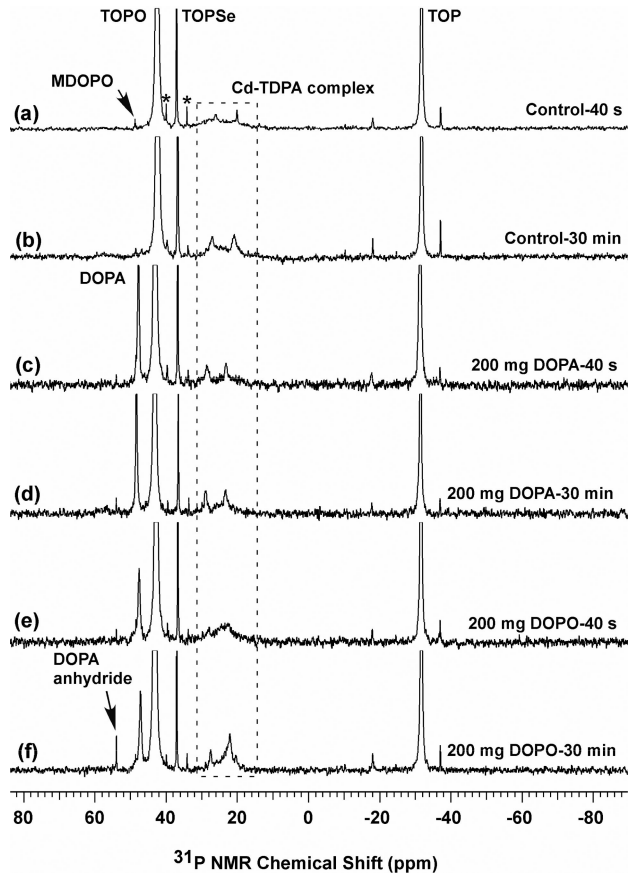


**Figure 3.**

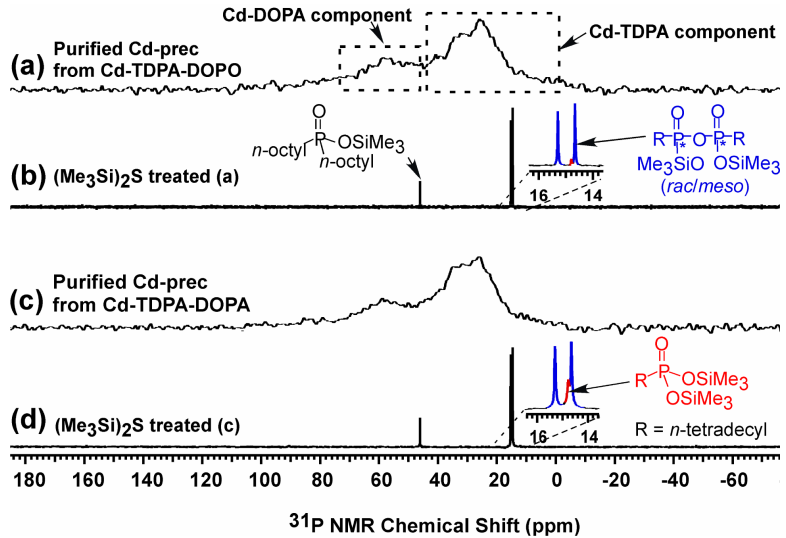
Representative TEM (a,d, and g) and HRTEM (b,c,e,f, and h) images of CdSe NCs grown (30-min reaction time) using the OA-and-TOPO protocol: control (no DOPA or DOPO added, a–c), with DOPA (200 mg, 0.69 mmol, d–f), and with DOPO (200 mg, 0.73 mmol, g and h). 90% TOP was used. The measured sizes ( $d \pm$  one standard deviation in  $d$  distribution) by TEM are: (a) 5.2 nm ( $\pm 15\%$ ), (d) 6.1 nm ( $\pm 25\%$ ), and (g) 4.2 nm ( $\pm 14\%$ ). The ZB segments of the NCs in the HRTEM images are highlighted in blue and the stacking faults or twinning planes are labeled as red lines.



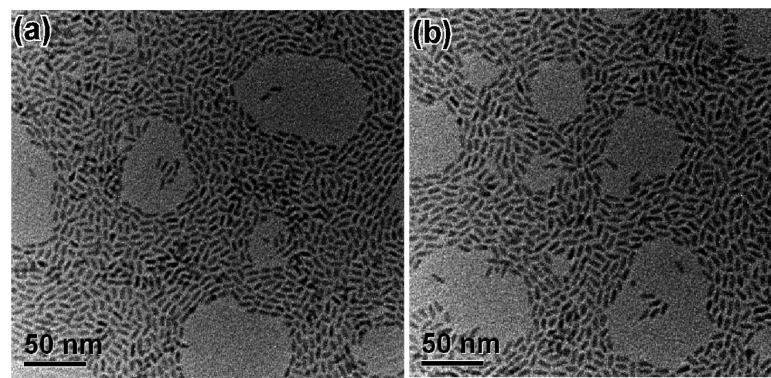
**Figure 4.**  
Temporal evolution of PL peak position (a), PL fwhm (b), and PL QY (c) of CdSe NCs grown using the OA-and-TOPO protocol with or without the addition of DOPA or DOPO.

**Figure 5.**

$^{31}\text{P}\{\text{H}\}$  NMR spectra (in  $d_8$ -toluene) of the reaction mixtures of CdSe NCs grown using the TDPA-and-TOPO protocol at 40-s and 30-min reaction times: control (a and b); with 200-mg DOPA (c and d), and 200-mg DOPO (e and f). 90% TOP was used. The peak intensities for TOPO ( $\sim 44$  ppm) were normalized. MDOPO (1-methylheptyl-di-*n*-octylphosphine oxide) is a TOPO isomer.<sup>42</sup> The asterisks label the  $^{77}\text{Se}$  satellites of TOPSe. Cd-TDPA complex represents Cd-*n*-tetradecylphosphonate complex and its signal may overlap with those of TDPA and TDPA anhydride. The assignments of DOPA, DOPA anhydride, and Cd-TDPA complex are provided in Figure S11 and in the text.

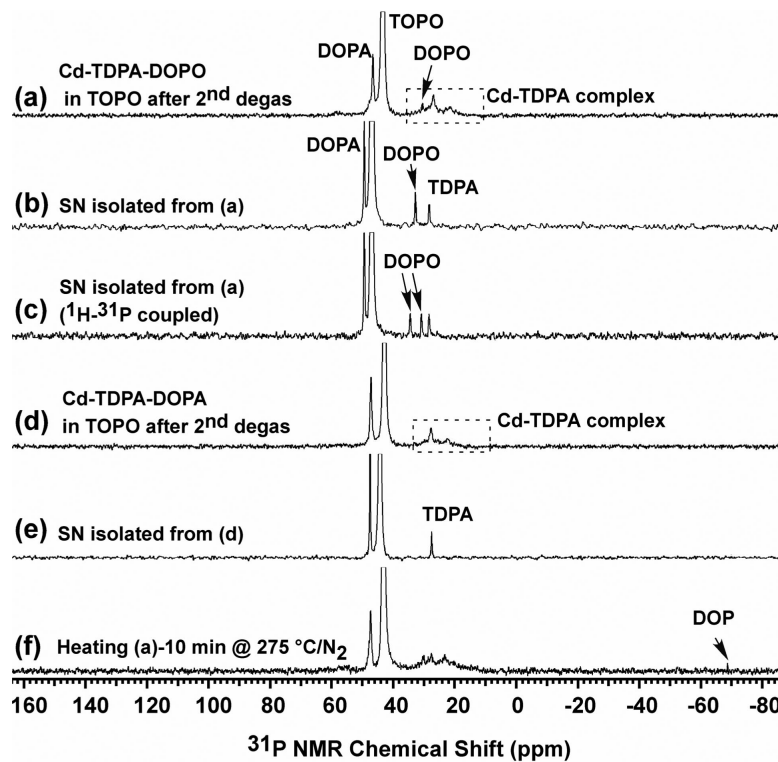
**Figure 6.**

$^{31}\text{P}\{\text{H}\}$  NMR spectra (in  $d_8$ -toluene) of the purified Cd precursors (a and c) and after their  $(\text{Me}_3\text{Si})_2\text{S}$  treatment (b and d). The Cd precursors were prepared using the TDPA-and-TOPO protocol with 200-mg DOPO (a) and 200-mg DOPA (c). Cd-DOPA represents Cd-di-*n*-octylphosphinate. The DOPA-derived *O*-(trimethylsilyl)-di-*n*-octylphosphinic acid (ODOPA, 46 ppm, see Figure S17 for confirmation), TDPA-derived *O,O'*-(trimethylsilyl)-*n*-tetradecylphosphonic acid (OTDPA, 14.8 ppm, labeled in red),<sup>54</sup> and the racemic and meso forms of TDPA anhydride-derived *O,O'*-(trimethylsilyl)-*n*-tetradecylphosphonic acid anhydride (OTDPA anhydride, 14.6 and 15.3 ppm, labeled in blue)<sup>54</sup> were identified (b and d).

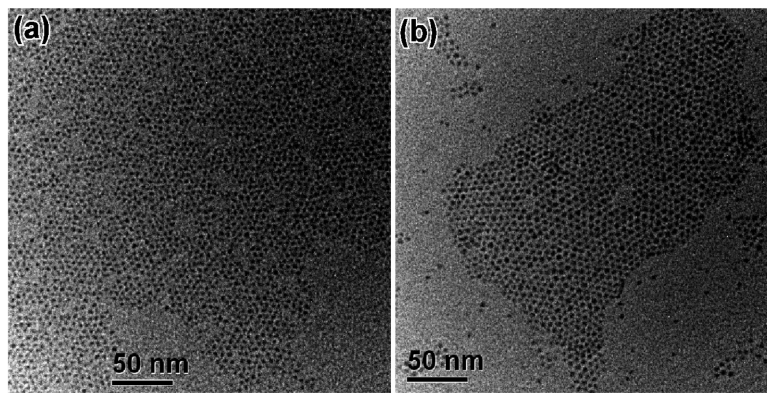


**Figure 7.**

Representative TEM images of CdSe NCs grown (30-min reaction time) using purified Cd precursors prepared from the TDPA-and-TOPO protocol with 200-mg DOPO (a) and with 200-mg DOPA (b). Purified TOPO was used as the solvent.

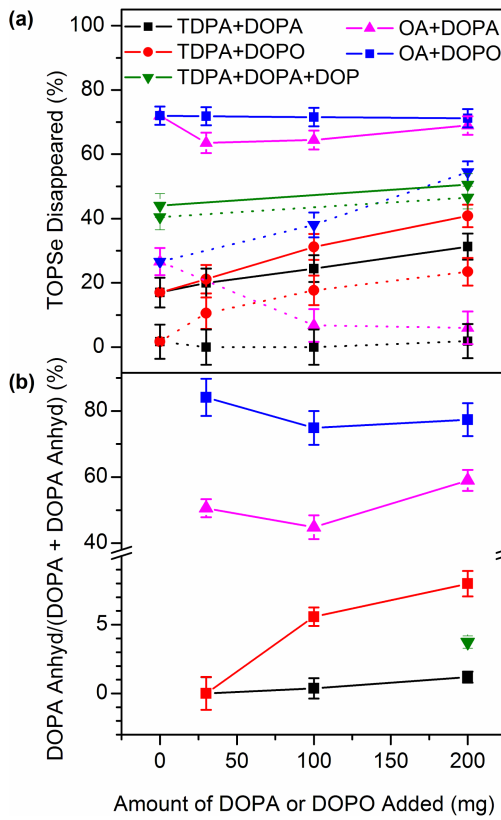
**Figure 8.**

$^{31}\text{P}\{\text{H}\}$  NMR spectra (in  $d_8$ -toluene) of the Cd-precursor mixtures made using the TDPA-and-TOPO protocol with 200-mg DOPO (a) and with 200-mg DOPA (d) after the second degassing process, their corresponding supernatants (SN) after the Cd-precursor isolations (b and e), and the Cd-precursor mixture of (a) being heated at 275 °C under  $\text{N}_2$  for 10 min (f). (c) is the  $^1\text{H}$ - $^{31}\text{P}$  coupled NMR spectrum of the SN in (b). Note the absence of DOP in (a).



**Figure 9.**

Representative TEM images of CdSe NCs grown (30-min reaction time) using the TDPA-and-TOPO protocol in the presence of (a) 22-mg DOP (without DOPA and DOPO added) and (b) 23-mg DOP and 200-mg DOPA.

**Figure 10.**

Precursor-conversion kinetics of the NC syntheses at 40-s (dotted traces) and 30-min (solid traces) reaction times. (a) Percentage (mol %) of TOPSe disappeared and (b) conversion (mol %) of DOPA into DOPA anhydride.

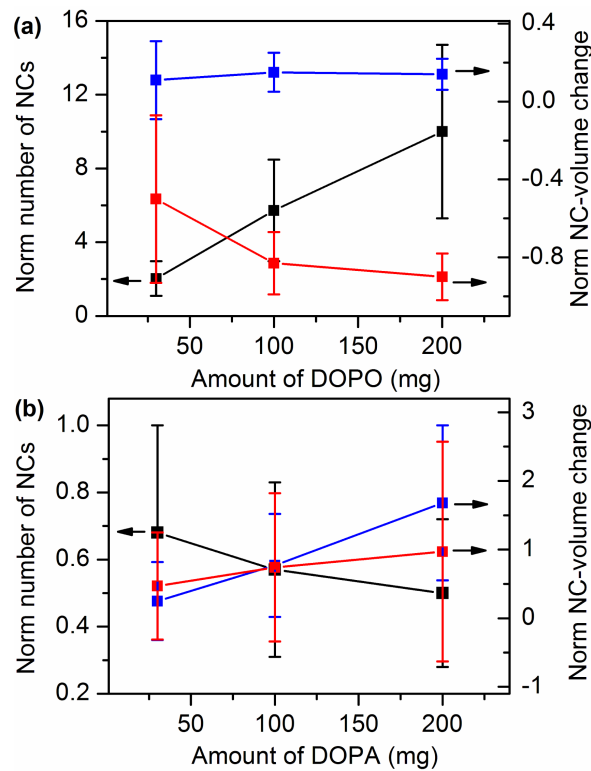


**Figure 11.**

Normalized number of NCs (black) and NC-volume change contributed from the change of the precursor conversion (blue) and that from the change of the number of NCs (red), as a function of the amount of DOPO (a) and DOPA (b) added. All data were normalized with respect to the control. The TDPA-and-TOPO protocol was used and the reaction time was 30 min. Detailed calculations are provided in Table S1 in the Supporting Information. The large error bars resulted from the NC volume calculations where we assumed  $\pm 10\%$  measurement errors in the  $d$  (and  $l$ ) of the NCs.